THE BELL SYSTEM TECHNICAL JOURNAL
Vol. 62, No. 5, May–June 1983
Printed in U.S.A.

An Experimental Broadband Imaging Feed

By T. S. CHU and R. W. ENGLAND*

(Manuscript received November 8, 1982)

Imaging with Fresnel diffraction taken into account is applied to the design of a broadband narrow pattern feed. This feed is not only a basic building block of an imaging beam waveguide, but also essential for an offset reflector antenna of large effective F/D ratio. Furthermore, it can be used as a constant beamwidth radiometer antenna for multifrequency remote sensing. We have built and tested a practical example that consists of an offset ellipsoidal reflector and a corrugated horn. Measured amplitude and phase patterns agree with calculated results, which include truncation effects. Systematic design procedures are obtained for a given feed horn and the required reflector illumination. Necessary and sufficient conditions of the thin lens model are translated into design parameters of an offset ellipsoidal reflector with projected circular aperture. Geometrical relations of the offset ellipsoid and calculations of radiation patterns are described in the appendices.

I. INTRODUCTION

The successful performance of an offset dual-reflector antenna often depends upon illumination by a broadband feed with a narrow feed pattern.[1] For example, a broadband corrugated horn with the required pattern could be used, but it would be excessively long for most practical applications. Good illumination can also be achieved by a narrowband offset launcher,[2] which is essentially an offset reflector fed by a relatively short feed horn. Excellent 19/28.5 GHz dual-frequency performance was demonstrated by the Crawford Hill 7-meter antenna using a quasi-optical frequency diplexer to combine two narrowband offset launchers.[1] However, this approach is not usually cost effective, especially for lower frequency systems. In this paper we present design

* Now at AT&T Long Lines.

procedures for *broadband* offset launchers and comparisons between calculated and measured patterns of both amplitude and phase. These feeds represent a considerable simplification of the hardware, and thus improve the prospect for system application of offset dual-reflector antennas.

The following analysis will assume the thin lens approximation for an imaging offset reflector. It will also make use of the frequency insensitivity of the field distribution in the aperture of a corrugated horn.[3,4] The principles of imaging have been discussed previously in connection with frequency-independent far-field beamwidths,[5] and the laws of geometrical optics have been used for the design of imaging reflector arrangements.[6] However, broadband feed illumination for reflector antennas needs not only constant beamwidth, but also constant phase center. The condition for satisfying the latter requirement is obtained in this paper by an interpretation of the additional phase shift[7] due to Fresnel diffraction. The imaging laws of geometrical optics are thus modified to provide a theoretically frequency-independent design of offset-launcher feeds. However, the practical bandwidth will be limited by the corrugated horn and truncation effects. These effects will be examined by numerical calculations and experimental measurements.

The imaging feed discussed here has important potential for application in radio communication and other scientific explorations. Furthermore, the basic properties of single-stage imaging are of vital interest in the design of multistage-imaging beam waveguides.[8] One notes the difficulty of performing pattern measurements of a bulky beam waveguide assembly. Both single- and double-stage imaging are also special cases of a proposed technique[9] for broadband astigmatic compensation in which the image of a corrugated horn through two astigmatic lenses can be designed to produce a specified astigmatic illumination.

Section II will discuss the imaging feed within thin lens approximation. Section III will describe how to translate the design parameters from the thin lens model to a practical offset ellipsoidal reflector with the required projected circular aperture. Section IV will give comparisons between calculated and measured data for both amplitude and phase patterns of an experimental broadband imaging feed. Geometrical relations of an offset ellipsoid and a calculation of radiation patterns will be given in Appendices A and B, respectively.

II. THIN LENS MODEL

It is well known that the aperture distribution of a corrugated horn with radius a_0 is the Bessel function $J_0\ (\alpha\rho/a_0)$.[3,4] The edge field vanishes when $\alpha = 2.405$. This normally occurs at the design frequency

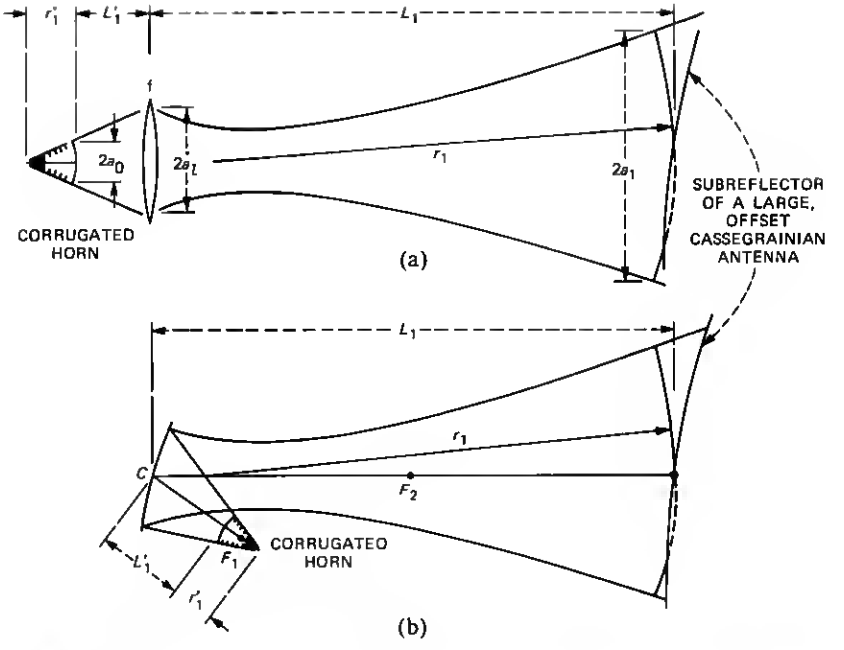

Fig. 1—Sketch of a broadband imaging feed. (a) Thin lens approximation. (b) Offset ellipsoidal reflector.

for resonant corrugations. However, α remains close to the above optimum value over a broad bandwidth if the aperture diameter is about five wavelengths or greater. If a magnified image of the corrugated-horn-aperture distribution is used to illuminate a reflector antenna, the illumination is expected to be a truncated Bessel function. For a specified reflector edge taper of T(in dB), the radius a_r of the illumination circle at the reflector aperture should have a value satisfying

$$20 \log_{10} J_o(\alpha a_r / a_1) = -T, \tag{1}$$

where $a_1 = Ma_0$ is the magnified corrugated-horn-aperture radius. The magnification is given by

$$M = \frac{L_1}{L_1'}, \tag{2}$$

where L_1 *and* L_1' are the distances of the illuminated reflector and the corrugated horn from the imaging lens, respectively, as shown in Fig. 1.

Now the focal length, f, of the imaging lens should obey the thin

lens formula:

$$\frac{1}{f}=\frac{1}{L_1}+\frac{L}{L_1'}. \tag{3}$$

Furthermore, the image-illumination phase-front radius of curvature r_1 can be expressed in terms of the feed-horn-aperture phase-front radius of curvature r_1' as

$$\frac{1}{r_1}=\frac{1}{L_1}\left[1+\frac{L_1'}{L_1}\left(1+\frac{L_1'}{r_1'}\right)\right]. \tag{4}$$

Equation (4), which is the same as the relation for Gaussian beam imaging,[8,9] is essentially an alternative form of eq. (7) in Ref. 7. This equation represents the additional phase shift due to Fresnel diffraction.

Equation (4) shows that r_1 will be always less than L_1 if all parameters on the right side are positive. r_1 may become greater than L_1 for negative r_1'. One notes that r_1' is always positive for any corrugated-feed horn unless modified by another lens or offset reflector. To obtain some feeling about the required physical spacings for a given pair of specified illumination and feed horn, normalized L_1 (with respect to r_1) has been plotted from eq. (4) versus normalized L_1' (with respect to r_1') for several ratios of L_1'/L_1 in Fig. 2. For a given pair of specified illumination and corrugated horn, i.e., L_1'/L_1, r_1 and r_1' specified, it is also convenient to rearrange eq. (4), as follows:

$$\frac{L_1}{r_1}=\frac{1+\dfrac{L_1'}{L_1}}{1-\left(\dfrac{L_1'}{L_1}\right)^2\dfrac{r_1}{r_1'}}. \tag{5}$$

It is of interest to note a few special cases of eq. (4). The near-field gregorian configuration[6] corresponds to $r_1'=\infty$ in eq. (4). J. A. Arnaud's confocal feed reflector arrangement[10] is also a special case in which $r_1'=-L_1'$ and $r_1=L_1$. However, Arnaud assumed both constant beamwidth and constant phase center for the corrugated horn to obtain a frequency-independent aperture distribution at his first reflector.

If the radiation from a corrugated horn is approximated by a Gaussian beam, the 1/e* beam radius at the horn aperture has been shown[5] to be $w_1'=0.64a_o$, where a_o is the horn-aperture radius. Then

* Here $e=2.71828$, whereas e represents eccentricity of a conic in the next section and appendices.

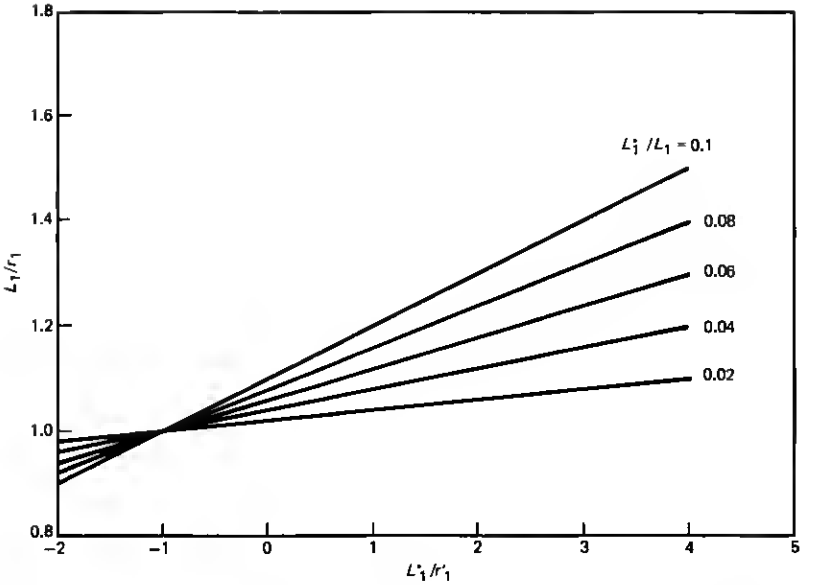

Fig. 2—Relation between image and object phase curvatures for various ratios of L_1'/L_1.

the Gaussian beam radius w_2 at the imaging lens can be found from[11]

$$w_2 = w_1' \sqrt{\left(\frac{L_1'}{r_1'} + 1\right)^2 + \left(\frac{\lambda L_1'}{\pi w_1'^2}\right)^2}. \tag{6}$$

The lens diameter should be 3.04 times the Gaussian beam radius w_2 for a truncation edge taper of −20 *dB*.

III. OFFSET ELLIPSOIDAL REFLECTOR WITH PROJECTED CIRCULAR APERTURE

In practice, the thin lens will be approximated by an offset ellipsoidal reflector, as shown in Fig. 1(b). The distances from the center of the reflector to the two foci, F_1 and F_2, are, respectively, the incident and reflected phase-front radii of curvature. The incident phase-front radius of curvature can be obtained from the Gaussian beam propagation formula[11]

$$R_1 = L_1 \Bigg/ \left[1 - \frac{\dfrac{L_1'}{r_1'} + 1}{\left(\dfrac{L_1'}{r_1'} + 1\right)^2 + \left(\dfrac{\lambda L_1}{\pi w_1'^2}\right)^2} \right]. \tag{7}$$

If the offset ellipsoid is in the far zone of the born, R_1 becomes the distance CF_1 from the phase center of the horn to the center of the reflector. The thin lens formula yields $R_2 = CF_2$, the reflected phase-front radius of curvature

$$\frac{1}{R_1} + \frac{1}{R_2} = \frac{1}{f}. \tag{8}$$

The frequency-dependent R_1 and R_2 are often not the same as L_1 and L_1' in eq. (3). The equivalent focal length f is identical to that in eq. (3). It has been shown[8] that the second-order terms of the offset ellipsoidal surface are only functions of f and the angle of incidence, whereas the third-order terms are also dependent upon R_1 and R_2.

The design of an offset ellipsoidal reflector with oversized aperture of rectangular shape was discussed in Ref. 8. Since corrugated feed horns and required reflector illuminations are often of circular shape, we shall now describe the design of offset ellipsoidal reflectors with projected circular apertures.

The intersection of an ellipsoid and a circular cone subtended at one focus is a plane ellipse subtended by another circular cone at the otber focus[1] (see Appendix A for proof and other geometrical relations). However, the two circular cone axes do not intersect the ellipsoid at the same point. In an ideal approximation of the thin lens by an offset ellipsoidal reflector, one would like to have both beam axes of the incident and reflected beams intersect the ellipsoid at the center of the offset reflector. This condition can be approximately realized by locating the intersection of R_1 and R_2 midway between the intersections 0 and 0′ of two circular cone axes with the ellipsoid, as shown in Fig. 3, i.e.,

$$R_1(\theta_{p1} - \theta_o) = R_2(\theta_o' - \theta_{p2}), \tag{9}$$

where

$$\frac{\sin \theta_{p1}}{\sin 2\theta_i} = \frac{R_2}{\sqrt{R_1^2 + R_2^2 - 2R_1R_2\cos 2\theta_i}} \tag{10}$$

and

$$\frac{\sin \theta_{p2}}{\sin 2\theta_i} = \frac{R_1}{\sqrt{R_1^2 + R_2^2 - 2R_1R_2\cos 2\theta_i}}. \tag{11}$$

θ_o and θ_o' are defined in Appendix A. We also need the expressions for the eccentricity, e, and the distance, f_o, between the vertex and tbe near focus:

$$f_o = \frac{|R_1 + R_2| - \sqrt{R_1^2 + R_2^2 - 2R_1R_2\cos 2\theta_i}}{2} \tag{12}$$

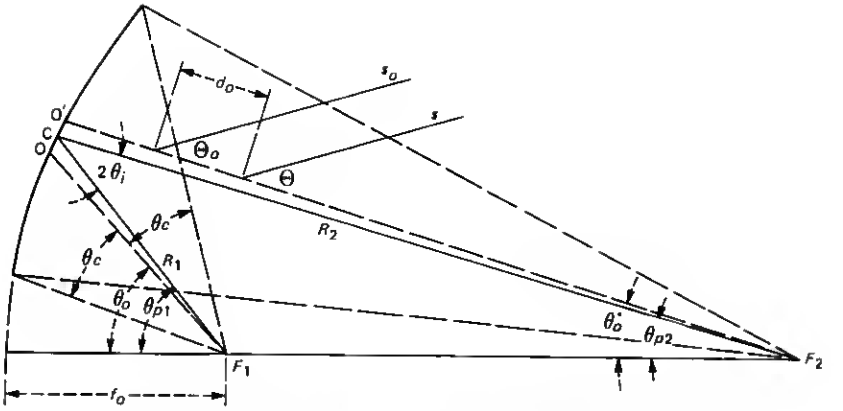

Fig. 3—Schematic diagram of an offset ellipsoidal reflector.

$$e = 1 - \frac{2f_o}{|R_1 + R_2|}. \tag{13}$$

Now the minor radius of the plane ellipse in eq. (23) should be equal to the radius of the projected circular aperture in the beam direction. (i.e., the thin lens aperture radius)

$$\rho_{\text{major}}\sqrt{1 - e^2\sin^2\theta_{po}} = a_l. \tag{14}$$

Substituting eqs. (20) and (22) into eq. (14), we obtain

$$e^2\cos^2\theta_o + 2e\cos\theta_c\cos\theta_o + 1 - \sin^2\theta_c\left[e^2 + \frac{(1+e)^2f^2}{a_l^2}\right] = 0. \tag{15}$$

When we are given an angle of incidence, θ_i, and a pair of radii of curvature, R_1 and R_2, eqs. (9) and (15) can be solved simultaneously for numerical values of θ_o *and* θ_c. These parameters completely determine both the shape and size of the ellipsoid.

IV. NUMERICAL AND MEASURED RESULTS

To demonstrate practical feasibility of the proposed imaging feed design, we have built and tested an experimental broadband offset launcher. This feed was designed to provide the illumination required for the hyperboloidal subreflector of the Crawford Hill 7-meter offset cassegrainian antenna.

Following the method of Section II, we obtain parameters for the thin lens model of this experimental feed, as listed in Table I. Using the procedures described in Section III, we translated the lens parameters into dimensions of an offset ellipsoid, as shown in the schematic diagram of Fig. 3. A design frequency of 22 GHz was used in eqs. (7) and (8) to find R_1 and R_2, as shown in Table II.

Table I—Design parameters of the thin lens model for a broadband imaging feed (all lengths are in cm.)

Required −15 dB illumination circle radius	47.5
Required phase-front radius of curvature	535.9
Frequency band (CHz)	19/28.5
Corrugated horn aperture radius, a_0	3.8
Horn apex to aperture distance, r_1'	15.9
Horn aperture to imaging lens distance, L_1'	47.5
Imaging lens to subreflector distance, L_1	684.6
Lens focal length, f	44.5
Lens radius (truncation edge taper ≈ 20 dB)	21
Lens to phase-center distance, Δ	148.7

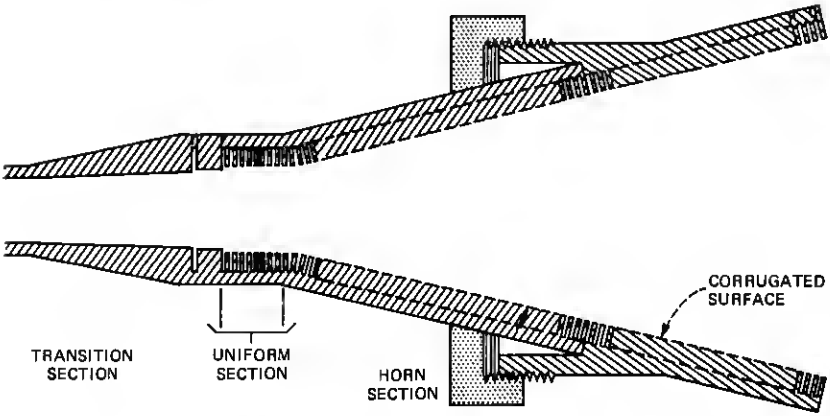

Fig. 4—Corrugated horn geometry.

A sketch of the corrugated horn is shown in Fig. 4. The corrugation depth is ahout a quarter wavelength at 18 GHz. The steps hetween smooth and corrugated sections help impedance matching hecause the desirahle HE_{11} mode in the corrugated guide is concentrated toward the center of the cross section. The return loss of the horn is better than 20 dB for frequencies ahove 16 GHz. The E- and H-plane heamwidths are nearly identical to each other from 16 to 30 GHz.

Figure 5 shows a photograph of the comhination of offset ellipsoidal reflector and corrugated horn. Amplitude and phase patterns have heen measured in hoth the offset plane and the transverse plane orthogonal to the offset. Since the phase center is located ahout 1.5 m from the center of the offset ellipsoid, physical rotation around the phase center would cause prohlems of mechanical unbalance. Therefore, the center of rotation in the pattern measurements is located midway hetween the ellipsoid and the phase center. The measured data can be transformed into measured patterns around the phase center hy the relations hetween the angles of rotation and between the path lengths.

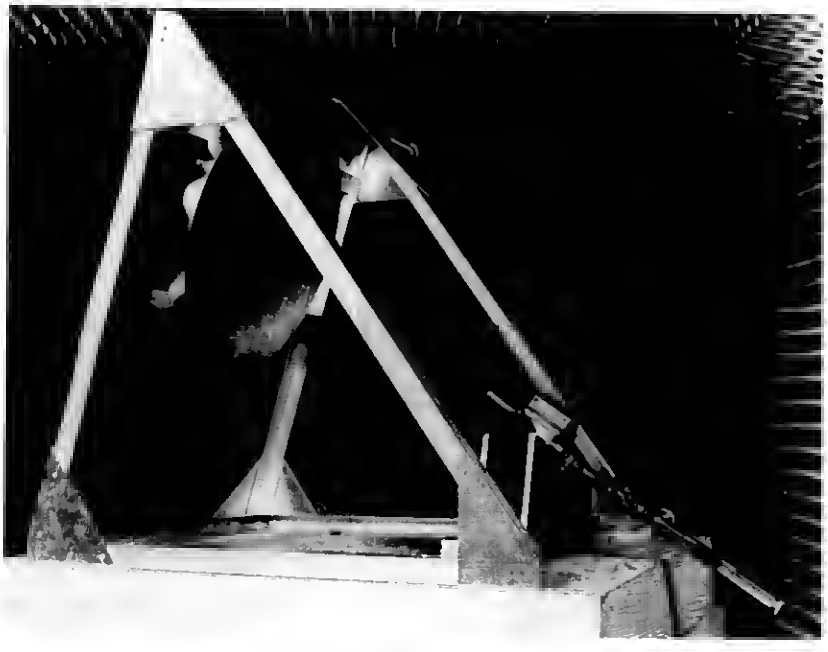

Fig. 5—Experimental broadband imaging feed.

Table II—Design parameters of the offset ellipsoidal reflector (all lengths are in cm.)

Incident phase-front radius of curvature R_1	54.36
Reflected phase-front radius of curvature R_2	244.22
Angle of incidence, θ_i	17°
Angle between incident center ray and major ellipsoidal axis, θ_{p1}	42.68°
Angle between reflected center ray and major ellipsoidal axis, θ_{p2}	8.68°
Offset angle, θ_o	41.87°
Half-cone angle, θ_c	22.09°
Offset angle at the distant focus, θ_o'	8.86°
Vertex to near focus distance, f_o	48.56
Eccentricity, e	0.67475
Semi-major-axis of plane ellipse, ρ_{major}	21.98
Semi-minor-axis of plane ellipse, ρ_{minor}	21
Semi-major-axis of ellipsoid, a	149.29
Semi-minor-axis of ellipsoid, b	110.18

The two equations below

$$\sin \Theta = \frac{s_o}{s} \sin \Theta_o \tag{16}$$

$$s = \sqrt{s_o^2 + d_o^2 - 2 s_o d_o \cos \Theta_o} \tag{17}$$

are similar to eqs. (32) and (31). The parameters are explained in Fig. 3. The angular conversion of eq. (16) will be required in both

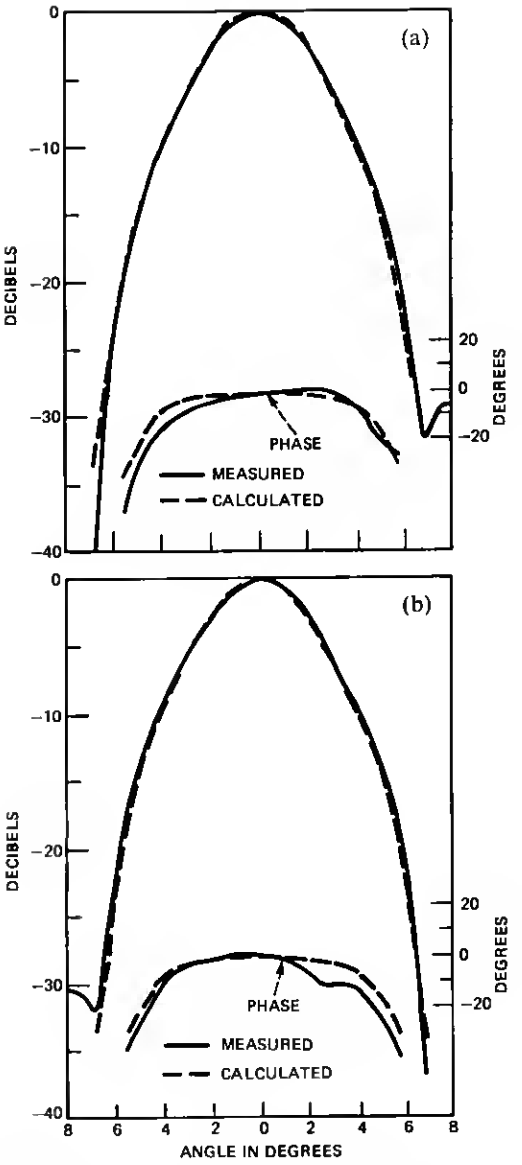

Fig. 6—19-GHz radiation pattern of transverse polarization (transverse perpendicular to offset) in (a) offset plane and (b) transverse plane.

amplitude- and phase-pattern transformations, whereas another factor of $(s + d_o - s_o)$ will be also added to the measured phase pattern.

To ensure reliable phase data, all pattern measurements were made in the azimuthal plane where a rotary joint can be used for avoiding

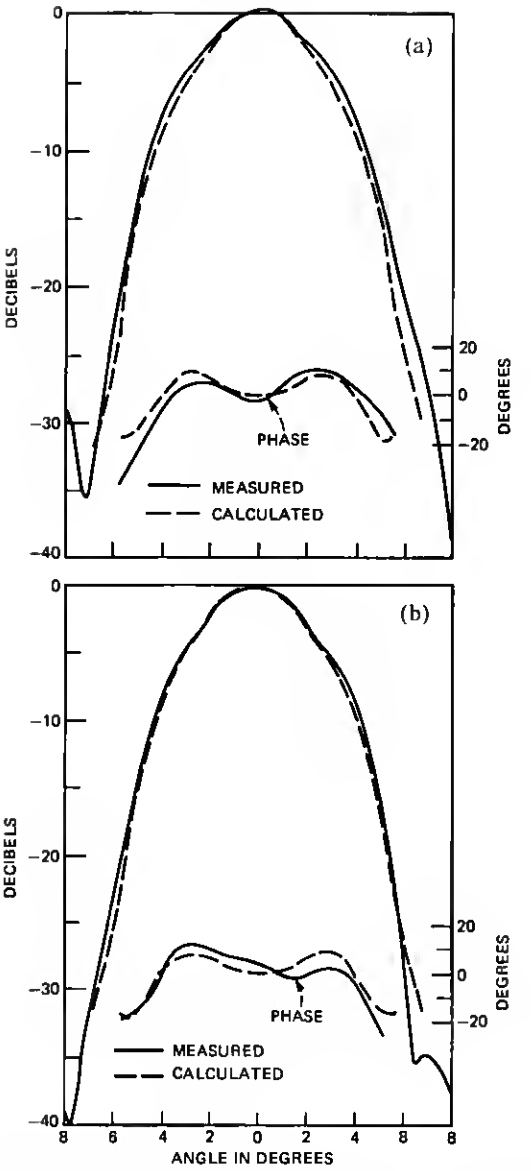

Fig. 7—23-GHz radiation pattern of transverse polarization (transverse perpendicular to offset) in (a) offset plane and (b) transverse plane.

cable motion during rotation of the turntable. Care was taken in keeping the same center of rotation by flipping over the feed assembly between measuring the transverse plane and offset plane cuts.

Calculations of radiation patterns are described in Appendix B. Both

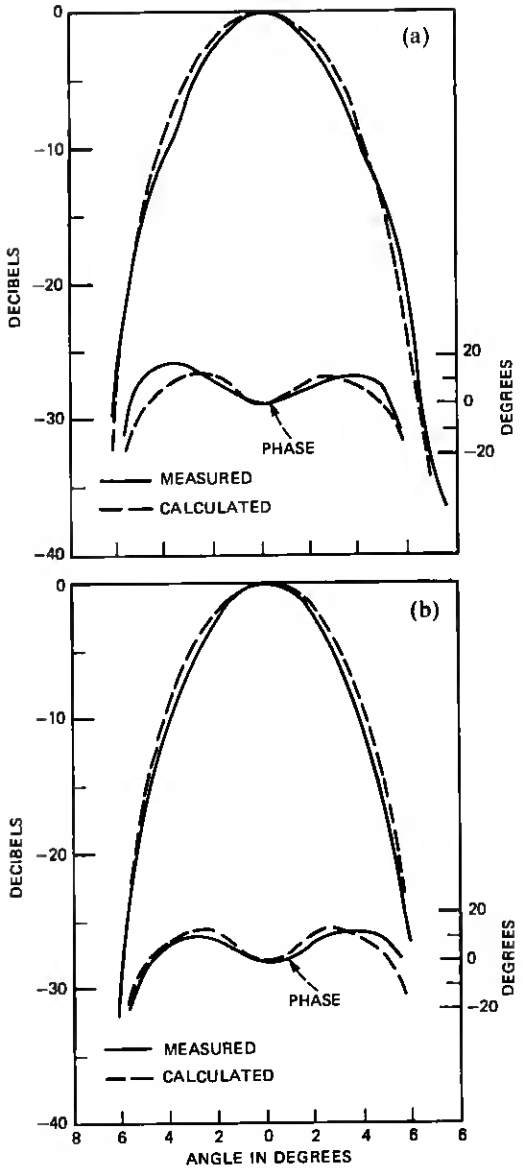

Fig. 8—28-GHz radiation pattern of transverse polarization (transverse perpendicular to offset) in (a) offset plane and (b) transverse plane.

measured and calculated patterns around the phase center are shown in Figs. 6, 7, and 8 for 19, 23, and 28 GHz, respectively. Comparisons between measured and calculated data show generally good agreement for both amplitude and phase patterns. An ideal imaging feed would

have a frequency-independent amplitude pattern of −15 dB taper at 5 degrees and a straight-line phase pattern that represents an exact spherical wave originating from a point source at the phase center. Deviations from these ideal patterns can be attributed to the imperfection of the paraxial approximation and to the truncation effect. Measured patterns also include the effect of deviation of the corrugated-horn-aperture field from the theoretical model. Figures 6 through 8 show that 28-GHz measured pattern widths are slightly narrower than those of 19 GHz. Phase deviations remain less than 20 degrees. These results are very similar to those of a long broadband corrugated horn designed for constant beamwidth feed.

The patterns in Figs. 6 through 8 were measured with the polarization transverse to the offset plane. Measurements with the polarization parallel to the offset plane showed similar patterns. Cross-polarized pattern measurements showed a maximum cross polarization of −26 dB, which is what would be expected from the offset geometry.[12]

V. DISCUSSIONS

Theoretical and experimental studies have demonstrated the feasibility of a broadband imaging feed using the combination of an offset ellipsoid and a corrugated horn. This feed is also important for serving as a basic building block of the imaging beam waveguide.

Since a broadband feed design will avoid the need of quasi-optical frequency diplexing, a much simpler, cost-effective feed system can be built to achieve performance similar to that of the 19/28.5 GHz feed of the Crawford-Hill 7-meter antenna.

The application of imaging of a corrugated horn by an offset ellipsoidal reflector is certainly not limited to broadband narrow feed patterns for large ground station antennas. For example, Dragone suggests[13] its application to terrestrial microwave repeater antennas. Furthermore, it can be used as a constant beamwidth radiometer antenna for multifrequency remote sensing.

REFERENCES

1. T. S. Chu et al., "The Crawford Hill 7-Meter Millimeter Wave Antenna," B.S.T.J., *57*, No. 5 (May–June 1978), pp. 1257–88.
2. M. J. Gans and R. A. Semplak, "Some Far-Field Studies of An Offset Launcher," B.S.T.J., *54*, No. 7 (September 1975), pp. 1319–40.
3. T. S. Chu and W. E. Legg, "Gain of Corrugated Conical Horns," IEEE Trans., *AP-30* (July 1982), pp. 698–703.
4. C. Dragone, "Reflection, Transmission, and Mode Conversion in a Corrugated Feed," B.S.T.J., *56*, No. 6 (July–August 1977), pp. 835–67.
5. C. Dragone, "An Improved Antenna for Microwave Radio System Consisting of Two Cylindrical Reflectors and a Corrugated Horn," B.S.T.J., *53*, No. 7 (September 1974), pp. 1351–77.
6. C. Dragone and M. J. Gans, "Imaging Reflector Arrangements to Form a Scanning Beam Using a Small Array," B.S.T.J., *58*, No. 2 (February 1979), pp. 501–15.

7. H. Kogelnik, "Imaging of Optical Modes—Resonators With Internal Lenses," B.S.T.J., *44*, No. 3 (March 1965), pp. 455–94.
8. T. S. Chu, "An Imaging Beam Waveguide Feed," IEEE Trans. AP-S, *AP-31*, No. 4 (July 1983).
9. T. S. Chu, "Broadband Astigmatic Compensation," Digest of 1981 IEEE Antenna and Propagation Symp., p. 131–4.
10. M. J. Gans, "Cross-Polarization in Reflector-Type Beam Waveguides and Antennas," B.S.T.J., *55*, No. 3 (March 1976), pp. 289–316.
11. T. S. Chu, "Geometrical Representation of Gaussian Beam Propagation," B.S.T.J., *45*, No. 2 (February 1966), pp. 287–99.
12. T. S. Chu and R. H. Turrin, "Depolarization of Offset Reflector Antennas," IEEE Trans., *AP*-21 (May 1973), pp. 339–45.
13. C. Dragone, private communication.
14. J. S. Cook, E. M. Elam, and H. Zucker, "The Open Cassegrain Antennas: Part I, Electromagnetic Design and Analysis," B.S.T.J., *44*, No. 7 (September 1965), pp. 1255–1300.
15. V. Jamnejad-Dailami and Y. Rahmat-Samii, "Some Important General Features of Conic-Section-Generated Offset Reflector Antennas," IEEE Trans., *AP*-28 (November 1980), pp. 952–7.

APPENDIX A

Geometry of Offset Ellipsoids

The geometrical properties of offset ellipsoids can be generalized from those[14] of offset paraboloids. The following formulas are derived by lengthy but straightforward algebra. The intersection of an offset ellipsoid and a circular cone subtended at the focus is a plane ellipse, which is subtended by another circular cone at the other (distant) focus. This property was indicated in Ref. 1, and also observed later in Ref. 15.

Let us define the ellipsoid in Figure 9 by

$$r = \frac{(1 + e) f_o}{1 + e \cos \theta_p}, \tag{18}$$

where the eccentricity, e, is less than unity. f_o is the distance between the origin in $X_p Y_p Z_p$ coordinates and the vertex, and θ_p is the polar angle with respect to the Z_p axis. We first find the intersection between the ellipsoid and the $x_o y_o$ plane, which is perpendicular to $x_p z_p$ plane, located at a distance r_o from the origin, and its normal makes an angle θ_{po} with the Z_p axis:

$$(1 - e^2 \sin^2\theta_{po}) \left\{ x_o - \frac{e(\sin \theta_{po})}{1 - e^2 \sin^2 \theta_{po}} [(1 + e) f_o - e r_o \cos \theta_{po}] \right\}^2 + y_o^2 = \frac{[e r_o \cos \theta_{po} - (1 + e) f_o]^2}{1 - e^2 \sin^2 \theta_{po}} - r_o^2. \tag{19}$$

Next, the following expressions are found for θ_{po} and r_o:

$$\theta_{po} = \sin^{-1} \left(\frac{\sin \theta_o}{\sqrt{1 + 2e \cos \theta_o \cos \theta_c + e^2 \cos^2 \theta_c}} \right) \tag{20}$$

$$r_o = \frac{(1 + e) f_o \cos \theta_c}{\sqrt{1 + 2e \cos \theta_o \cos \theta_c + e^2 \cos^2 \theta_c}}, \tag{21}$$

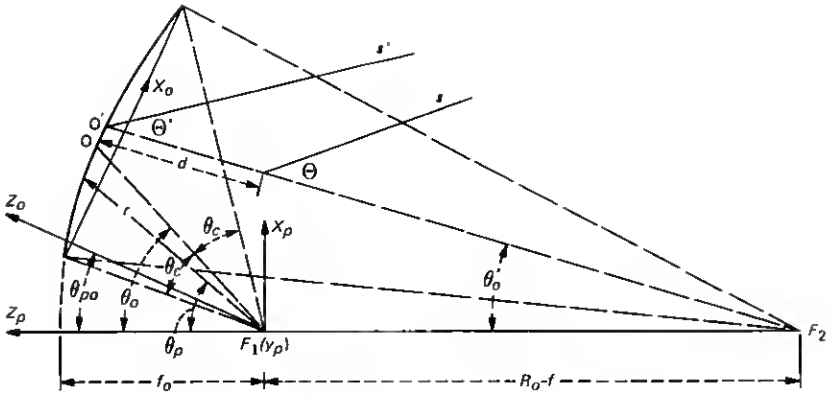

Fig. 9—Geometry of an offset ellipsoid subtended by circular cones at two foci.

where $\theta_o + \theta_c$ and $\theta_o - \theta_c$ are the polar angles of the top and bottom edges of the offset ellipsoid in the $x_p z_p$ plane. Now it can be shown that the intersection of the $x_o y_o$ plane with the circular cone, which has its axis oriented at $\theta_p = \theta_o$ and a half cone angle of θ_c, is the same ellipse as represented by eq. (19).

The major and minor radii of the ellipse are

$$\rho_{\text{major}} = \frac{(1 + \text{e}) f_o \sin\theta_c \sqrt{1 + 2e\cos\theta_o\cos\theta_c + e^2\cos^2\theta_c}}{1 + 2e\cos\theta_o\cos\theta_c + e^2\cos^2\theta_c - e^2\sin^2\theta_o} \tag{22}$$

$$\rho_{\text{minor}} = \rho_{\text{major}}\sqrt{1 - e^2\sin^2\theta_{po}}. \tag{23}$$

When $e = 1$, the above equations are reduced to those of Appendix A in Ref. 14. One notes an error in eq. (50) for the plane ellipse in Ref. 14, i.e., missing a term $(r_o \tan\theta_{po})$ in the bracket on the left-hand side of that equation.

The axis of the circular cone subtended at the second (distant) focus is oriented with respect to the major axis of the ellipsoid at

$$\theta'_o = \frac{1}{2}\left\{\sin^{-1}\left[\frac{r_2}{R_o + f_o - r_2}\sin(\theta_o + \theta_c)\right] + \sin^{-1}\left[\frac{r_1}{R_o + f_o - r_1}\sin(\theta_o - \theta_c)\right]\right\}, \tag{24}$$

where

$$r_{1,2} = \frac{(1 + \text{e}) f_o}{1 + \text{e}\cos(\theta_o \mp \theta_c)} \tag{25}$$

are the radial distances from the (near) focus to the termini of the major axis of the ellipse represented by eq. (19) and

$$R_o = f_o\left(\frac{1+\mathrm{e}}{1-e}\right) \tag{26}$$

is the distance from the vertex to the second focus.

APPENDIX B

Calculation of Radiation Pattern

In this appendix we shall calculate tbe radiation pattern of an offset ellipsoid illuminated by a corrugated feed horn. The numerical integration of the diffraction integral accomplishes computer simulation of the hardware.

When an ellipsoid is illuminated by a feed located at the near focus, the geometrical optic rays reflected from the ellipsoid are expected to converge toward the distant focus. Although the diffraction effect will take place before reaching that second focus, the ray approximation should be valid in the vicinity of the ellipsoid. To find the radiation from the ellipsoid, we will employ a spherical wave field in an equivalent plane aperture that is perpendicular to tbe axis of, and subtended by, the cone of reflected rays, and passes through the point, O′, of intersection of the centric reflected ray with the ellipsoid. The radius of curvature of the spherical wave is the distance, R_o', from the distant focus to the point O′.

$$R_o' = \frac{(1+\mathrm{e})f_o}{1 - e\cos\theta_o'} \tag{27}$$

The transverse cartesian coordinates in the plane aperture are

$$\begin{cases} x = R(\cos\theta_o\sin\theta\cos\phi + \sin\theta_o\cos\theta)\cos\theta_o' \\ \qquad - [R(-\sin\theta_o\sin\theta\cos\phi + \cos\theta_o\cos\theta) + R_o - f]\sin\theta_o' \\ y = R\sin\theta\sin\phi, \end{cases} \tag{28}$$

where

$$R = \frac{(1+\mathrm{e})f_o}{1 + \mathrm{e}(\cos\theta_o\cos\theta - \sin\theta\sin\theta_o\cos\phi)} \tag{29}$$

is the position radius from the focus to the ellipsoid. θ and ϕ are the standard spherical coordinates with the polar axis F_1O along the axis of the circular cone subtended at the near focus, as shown in Fig. 9.

Using a small angle scalar approximation, we can determine the radiation of the offset ellipsoid as

$$E = \frac{j\mathrm{e}^{-jk(s+d)}}{\lambda(s+d)}\int\frac{F}{R}\exp\left\{jk\left[x\sin\Theta'\cos\Phi + y\sin\Theta'\sin\Phi + \frac{x^2+y^2}{2R_o'} - \frac{x^2+y^2}{2(s+d)} + (s+d-s')\right]\right\}dA, \tag{30}$$

where F is the feed pattern, which will be described later. The term $(x^2 + y^2)/2(s + d)$ is a phase correction needed for tbe Fresnel region in which the Cassegrainian subreflector is located. The factor $(s + d - s')$ is added to give a phase pattern with respect to the phase center, which is located at a distance d in front of tbe ellipsoid. s is the distance between the phase center and the field point, and s' is the distance between the point O′, which is the effective center of the ellipsoid aperture, and the field point

$$s' = \sqrt{s^2 + d^2 + 2sd\cos\Theta}. \tag{31}$$

The angle Θ', between s′ and the cone axis $O'F_2$, is related by the sine law to the angle Θ between s and the cone axis, as shown below:

$$\sin\Theta' = \frac{s}{s'}\sin\Theta. \tag{32}$$

ϕ is the azimuth coordinate of the field point. The surface element dA is

$$dA = \frac{R^2\sin\theta d\theta d\phi}{\cos\theta_i}\cos\theta_r, \tag{33}$$

where θ_i is the angle of incidence between the incident ray and the unit vector normal to the ellipsoidal surface, and θ_r is the angle between this unit normal and the beam axis. Since the ellipsoids under consideration are only slight perturbations of paraboloids, $\cos\theta_i \approx \cos\theta_r$. Noting the symmetry of the aperture field, eq. (30) becomes

$$E = \frac{je^{-jk(s+d)}}{\lambda(s+d)}\int_o^{\pi}\int_o^{\theta_c} F\exp jk\left[x\sin\Theta'\cos\Phi + \frac{x^2+y^2}{2R_o'} - \frac{x^2+y^2}{2(s+d)} + (s+d-s')\right]\cos[ky\sin\Theta'\sin\Phi]R\sin\theta d\theta d\phi. \tag{34}$$

The feed pattern of a corrugated horn is given by

$$F(\Theta') = \int_0^1 J_o(\alpha r)J_o\left(ka\sin\theta'\frac{R}{R'}r\right)e^{-jk\left[ar^2\tan\frac{\beta}{2} + \frac{(ar)^2}{2R'} + \ell(1-\cos\theta')\right]}rdr, \tag{35}$$

where a is the aperture radius, β is the half cone angle of the horn, $\alpha = 2.405$ for frequencies close to the resonance of the corrugated depth, r is the normalized radial coordinate of the horn aperture, and $\sin\theta'$ is multiplied by R/R' because θ' is referred to the ellipsoid focus (the phase center of the horn), which is located at a distance ℓ behind the horn aperture. R' is the distance from the center of the horn aperture to a point on the ellipsoid:

$$R' = \sqrt{R^2 + \ell^2 - 2R\ell\cos\theta'}. \tag{36}$$

The first term $kar^2\tan(\beta/2)$ in the exponential bracket of eq. (35) is the phase deviation in the horn aperture, the second term is a phase correction in the Fresnel region, and the third term is added to give a phase pattern with respect to the horn phase center (ellipsoidal focus) instead of the horn aperture.

To compensate for the difference in length between the radii from the focus toward the top and bottom edges of the offset ellipsoid, the axis of the feed horn is offset by an angle θ_1 from the axis of the circular cone subtended by the ellipsoid at the focus. θ' can be expressed in terms of the angular coordinates (θ, ϕ) of the offset ellipsoid:

$$\cos\theta' = \cos\theta\cos\theta_1 + \sin\theta\sin\theta_1\cos\phi. \tag{37}$$

$\theta_1 = 1.6$ degrees is used in the calculated patterns of Figs. 6, 7, and 8.